Structural and Multidisciplinary Optimization (2018) 58:2253–2268
https://doi.org/10.1007/s00158-018-2014-3

INDUSTRIAL APPLICATION

Optimized vibro-acoustic design of suspended glass panels

Roberto Aiello[1,2] · **Fabio Auriemma**[1]

Received: 30 December 2017 / Revised: 11 May 2018 / Accepted: 17 May 2018 / Published online: 26 June 2018

Abstract

Suspended glass panels are monolithic or laminated frameless windows sustained by a number of holders, typically located in the vicinity of the edges. These panels can be used, among other purposes, as noise barriers. The vibro-acoustic behaviour of glass windows is critical at low frequencies, where the problem is often tackled by increasing the thickness, thus the mass, of the panels. As a consequence, solutions which preserve low mass are greatly sought by industries. In this study, the vibro-acoustic behaviour of different suspended glass panels is addressed. An optimization procedure is implemented, aiming at finding the position of the holders which maximizes the acoustic transmission loss (TL) averaged at low- and very low-frequency ranges. First, an iterative procedure, based on comparison of experimental and numerical modal data, has been implemented to extract the material properties (Young's modulus and Poisson's ratio) of the panels. Second, these properties have been used in an optimization procedure based on finite difference approximation of the objective function, the averaged transmission loss. The vibro-acoustic analyses, required by the optimization procedure, have performed by means of hybrid finite element method/statistical energy analysis (FEM/ SEA). 16 different design cases have been considered in the optimizations, i.e. 2 different frequency ranges (20-300 Hz and 20-1000 Hz), 2 panel geometries (square 1m x 1m and rectangular 2.5m x 0.8m), 2 constitutive material properties (monolithic tempered glass and laminated tempered glass) and 2 mounting solutions (4 and 6 holders). The transmission losses of the optimized and the standard configurations, where the holders are placed close to the edges, are compared.

Keywords Laminated glass · Suspended glass panels · Glass windows · FEM/SEA · Optimization

1 Introduction

The use of optimization techniques for the design of structures with enhanced vibro-acoustic behaviour can be found in a number of literature articles (Joshi et al. 2015; Bös 2006; Nandy and Jog 2012; Tinnsten and Esping 1999; Bös 2006; Chavan and Manik 2010; Joshi et al. 2015; Nandy and Jog 2012; Tinnsten 2000; Tinnsten and Esping 1999; Zargham et al. 2016; Esping 1995; Bös 2006; Belegundu et al. 1994). For instance, in the work Joshi et al. (2015) the panel mass and the radiated acoustic power of a stiffened panel have been minimized in a multi-objective optimization approach. In Bös (2006), the acoustical properties of structures, including plates, are improved by finding the optimized thickness distribution. In Nandy and Jog (2012), minimizing the dynamic compliance of the structure has been shown to indirectly benefit the sound power levels radiated by the structure.

The present paper addresses the optimization problem of maximizing the sound transmission loss of *suspended panels*, averaged in low- and very low- frequency ranges (20-300 Hz and 20-1000 Hz, respectively). In fact, theoretical studies have shown that the insulation at low-frequencies is mass-controlled, thus intrinsically more challenging to achieve and critical for the human comfort (Beranek and Work 1949; Auriemma 2017). This motivates the ranges of investigation selected in this paper.

The design parameters of the optimization problem are the positions of the holders used to support the panels, which have great impact on the vibro-acoustic behaviour

Responsible Editor: Jianbin Du

✉ Fabio Auriemma
fabio.auriemma@ttu.ee

Roberto Aiello
roberto.aiello@ino.cnr.it

[1] Department of Mechanical and Industrial Engineering, Tallinn University of Technology, Ehitajate tee 5, z.i.p. 19086, Tallinn, Estonia

[2] Present address: Consiglio Nazionale delle Ricerche, Istituto Nazionale di Ottica, Via Campi Flegrei, 34, z.i.p. 80078, Pozzuoli, Italy

Fig. 1 Suspended glass panels utilized as external walls for a lift system in Tallinn University of Technology. **a** Global view. **b** View of one of the rectangular suspended panels of the façade

of the panels. Being the suspended panels widely utilized solutions with both aesthetic and functional purposes (see Fig. 1), the problem addressed in this paper is of interest for modern architectural and civil engineering applications.

We remind here that the sound transmission loss of a partition is defined as a function of the transmission factor τ:

$$TL = 10 \log \left(\frac{1}{\tau} \right) \tag{1}$$

where τ is the ratio of the transmitted (P_t) over the incident power (P_i) and represents the fraction of the acoustic power transmitted throughout the partition. τ is strictly related to the vibrational behaviour of the partition.

There is a vast number of theoretical studies about the sound transmission loss of different types of acoustic partitions: perfectly limp plates (Cremer 1942), combinations of impervious layers, air gaps and acoustical blankets in

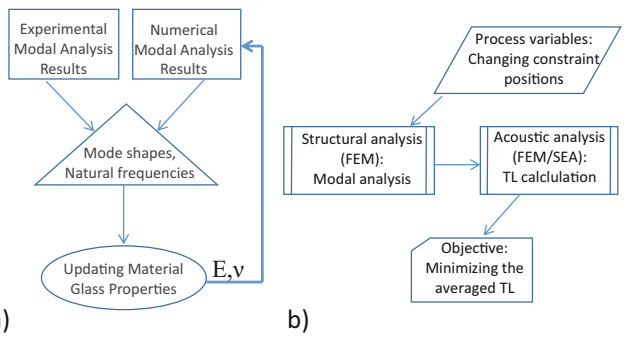

Fig. 2 2-step procedure implemented in this study. **a** Material characterization; **b** Optimization

Table 1 Panel configurations examined in this work

Case	Shape	Nr. of mountings	Panel structure	Freq. range [Hz]
1	Square	4	Monolithic	20-300
2	Square	4	Monolithic	20-1000
3	Square	4	Laminated	20-300
4	Square	4	Laminated	20-1000
5	Square	6	Monolithic	20-300
6	Square	6	Monolithic	20-1000
7	Square	6	Laminated	20-300
8	Square	6	Laminated	20-1000
9	Rectangle	4	Monolithic	20-300
10	Rectangle	4	Monolithic	20-1000
11	Rectangle	4	Laminated	20-300
12	Rectangle	4	Laminated	20-1000
13	Rectangle	6	Monolithic	20-300
14	Rectangle	6	Monolithic	20-1000
15	Rectangle	6	Laminated	20-300
16	Rectangle	6	Laminated	20-1000

normal incidence (Beranek and Work 1949) or diffuse acoustic field (London 1950), infinite panels (Mulholland et al. 1967), finite partitions (Fahy 1985), thin or tick panels (Munjal 1993), single- or multi- layered structures (Laurikis et al. 1992; Ookura and Saito 1978; Bolton et al. 1996; Panneton and Atalla 1986). In most of the literature studies, finite partitions are examined mainly in simply supported or clamped configurations.

In the present paper, the transmission loss of the panels has been computed by means of numerical methods. In fact, due to the complexity of the boundary conditions related to the presence of the holders, analytical solutions would be challenging to achieve and unwieldy. For this reason, a numerical approach based on hybrid finite element/statistical energy analysis has been used, where the statistical energy analysis utilizes the modal data of the panels obtained by means of finite element method (Maxit and Guyader 2001b; Stelzer et al. 2010) (see Fig. 2b). In the acoustical simulations, the panels are considered in baffled configuration, under diffuse field of excitation.

The optimization process presented here relies on an Eulerian approach, where each panel is discretized with the same fixed mesh in all numerical analyses involved in the process (Sigmund and Maute 2013). As a consequence, different holder positions are represented by different sets of fully constrained nodes. The optimization algorithm is based on finite difference. With this method, an approximate value of the gradient of the objective function in a certain point (i.e. for a certain set of holder positions) is calculated by using the values computed on the discrete

domain in the neighbourhood of that point. This allows to easily detect directions of steepest variation of the objective function. As pointed out in Sigmund (2011), a gradient based approach is usually preferable in this type of problems.

Different panel geometries, number of mountings and layer configurations have been taken into account for both 20-300 Hz (very low-) and 20-1000 Hz (low-) frequency ranges. Specifically, square and rectangular panels, 4 and 6 discrete mountings, monolithic tempered and laminated tempered glass panels with an intermediate layer of polymeric film (Polyvinil Butiral – PVB), summing up to a total of 16 different configurations (see Table 1).

Preliminarly, the suspended panels are studied by identifying some of the material properties not known a-priori. This is done by means of a classical procedure based on comparison of experimental and numerical modal data (Siano et al. 2015) (see Fig. 2a).

2 Material characterization procedure

As previously mentioned, a two-step procedure has been implemented in this paper to first characterize the materials and then to optimize the performance of the panels (see Fig. 2).

In the first step, the material properties used in a FEM modal analysis of glass samples have been varied until the experimental modal results are matched. The final values describe the actual properties with a level of approximation which is satisfactory for the purposes of this paper.

This approach provides linear elastic isotropic homogenized material properties also for the laminated samples with PVB layer. The assumption of linear elasticity is compatible with the constitutive laws and with the small displacement hypothesis underlying the linear vibro-acoustic analysis. On the other hand, the homogenization of the properties of laminated samples allows to model the two constituting materials as if they were one with equivalent mechanical characteristics. It will be shown that Young's modulus and Poisson's ratio extracted for the laminated sample are in agreement with the values found in literature. These values are higher than in case of monolithic sample, which shows an increase of resistance to the longitudinal and transverse deformations.

The experimental and numerical methodologies involved in the material characterization procedure are summarized in the two following sub-sections.

2.1 Modal analysis with response model

When a structure is excited by a set of sinusoidal forces provided with with individual frequencies, amplitudes and phases, it is possible to write the forced response equation, that is:

$$\{X\} = \left([K] - \omega^2 [M] + \omega [C]\right)^{-1} \{F\} \tag{2}$$

where ω is the angular velocity of the force, $[K]$ is the stiffness matrix, $[M]$ is the mass matrix, $[C]$ is the damping matrix, $\{F\}$ and $\{X\}$ are Nx1 vectors of time-independent complex amplitudes representing forcing and displacements, respectively. The general element in the Frequency Response Matrix (FRF), $H_{jk}(\omega)$, is defined as:

$$H_{jk}(\omega) = \left(\frac{X_j}{F_k}\right); F_m = 0; m \neq k \tag{3}$$

An efficient way to determine the FRF parameters makes use of the modal properties of the system. In this case, the generic element of the FRF matrix, $H_{jk}(\omega)$, becomes

$$\begin{aligned} H_{jk}(\omega) &= \sum_{r=1}^{n} \frac{\phi_j^{(r)} \phi_k^{(r)}}{\omega_r^2 - \omega^2 + i\omega 2\nu\omega_r} \\ &= \sum_{r=1}^{n} \frac{A_{jk}^{(r)}}{\omega_r^2 - \omega^2 + i\omega 2\nu\omega_r} \end{aligned} \tag{4}$$

where r is the number of the mode shapes or degrees of freedom, terms $\phi_{j,k}^{(r)}$ are the mass normalized eigenvector components, $A_{jk}^{(r)}$ are the products of the mass-normalized eigenvector components (named modal constants), ω_r is the natural frequency, $\nu = c/2\sqrt{mk}$ is the modal damping (Edwins 2003).

The general process of the experimental modal analysis aims at finding the modal parameters, ω_r, ν and $A_{jk}^{(r)}$ (thus $\phi_{j,k}^{(r)}$), appearing in a theoretical expression of FRF of the type of (4), which allows to better approximate the experimental FRF.

There are several techniques to extract the modal parameters. In this work, the *peak-picking* method has been used (Edwins 2003). It belongs to the class of methods based on the "single degree of freedom" (SDOF) hypothesis. These methods assume that, in the vicinity of a natural frequency of mode r^*, the terms of (4) with $r \neq r^*$ sum up to a constant term $B_{ij}^{(r^*)}$ which is approximately independent from frequency and the (4) becomes:

$$H_{jk}(\omega \approx \omega_{r^*}) = \frac{A_{jk}^{(r^*)}}{\omega_{r^*}^2 - \omega^2 + i\omega 2\nu\omega_{r^*}} + B_{jk}^{(r^*)} \tag{5}$$

In particular, the peak-picking method assumes that the term $B_{ij}^{(r^*)}$ is negligible. In this case, the (5) at $\omega = \omega_{r^*}$ reduces to:

$$H_{jk}(\omega_{r^*}) = \frac{A_{jk}^{(r^*)}}{i\omega 2\nu\omega_{r^*}} \tag{6}$$

so that $|H_{jk}(\omega_{r^*})| = A^{(r^*)}/\left(2\nu\omega_r^2\right)$. The peak-picking method is applied by first detecting the individual resonance

Table 2 Experimental natural frequencies and damping ratios

Mode number	Monolithic sample [Hz]	Modal damping (monolithic)[%]	Laminated sample [%]	Modal damping (laminated)[%]
1	172	0.42	185	0.96
2	265	0.87	271	2.61
3	477	0.20	497	1.54
4	569	0.35	573	2.26
5	944	0.19	928	2.55

peaks on the FRF plot, the frequencies of the maxima representing the natural frequencies ω_{r^*}. Once a local maximum of the FRF is detected, $|H|$, the frequency bandwidth delimited by the response level, $|H|/\sqrt{2}$, is determined. Thus, the two "half-power" points ω_a and ω_b are intercepted at $|H|/\sqrt{2}$. Finally, the damping of the mode is estimated as $\nu = \left(\omega_a^2 - \omega_b^2\right)/4\omega_{r^*}^2$.

Once ω_{r^*} and ν have been obtained, it is possible to extract the mode shape $\phi_j^{(r^*)}$ by using the term $H_{jj}(\omega_{r^*}) = \phi_j^{(r^*)}\phi_j^{(r^*)}/(i\omega 2\nu\omega_{r^*})$, which is the frequency response function obtained by hitting the point where the accelerometer is located. Finally, the other $\phi_k^{(r^*)}$ modes are deduced by using the terms $H_{jk}(\omega_{r^*})$.

The peak-picking method works adequately when the following conditions are met: the frequency response function of the structure exhibits well separated modes; the modes are not so lightly-damped, otherwise accurate measurements at resonance are difficult to obtain; the modes are also not so heavily damped, otherwise the response at a resonance is strongly influenced by more than one mode. These conditions are met in the case of panels studied here. In fact, the damping values do not overcome 3%, so the peaks considered are all sharp peaks. Moreover, the natural frequencies are spaced apart at least 76 Hz in the first 5 modes (see results in Table 2). It must be also pointed out that the errors related to the modal amplitudes, sometimes involved in the use of the peak-picking, does not influence the material characterization process since this process relies on experimental-numerical comparisons of eigenvalues rather than eigenvectors. An estimate of the error on the natural frequencies is ±5 Hz resulting in a variation of ±2% on the material properties identified.

2.2 Modal analysis with finite elements

The other methodology, used in combination with the experimental modal test to extract the material properties of the samples, is the Finite Element Method (Siano et al. 2016, 2010; Rämmal and Lavrentjev 2008).

The FEM has been used to solve the discrete motion free equation, Zienkiewicz and Taylor (2000):

$$[M]\{\ddot{x}(t)\} + [K]\{x(t)\} = \{0\} \tag{7}$$

In a weak formulation, the mass matrix $[M]$ and the stiffness matrix $[K]$ are expressed as:

$$[M_i] = \int_{\delta\Omega} [N_i]\rho[N_i]^t \delta\Omega \quad [K_i] = \int_{\delta\Omega} [B_i]^T [C][B_i]\delta\Omega \tag{8}$$

In the (8) the integrals are evaluated for each element i of volume $\delta\Omega$ and then assembled by means of a proper procedure, Petyt (1998). $[N_i]$ is the shape function matrix of the element i, ρ is the density, $[B_i] = \delta[N_i]/\delta x$ is the strain displacement matrix of the same element and [C] is the stress-strain (elasticity) matrix related to the material properties, including Young's modulus (E) and Poisson's ratio (ν). [C] relates the stress $[\sigma]$ and strain $[\epsilon]$ tensors through the Hooke's law, $[\epsilon] = [C][\sigma]$. For linear elastic homogeneous isotropic material this relationship yields to:

$$\begin{bmatrix} \epsilon_{xx} \\ \epsilon_{yy} \\ \epsilon_{zz} \\ \epsilon_{yz} \\ \epsilon_{zx} \\ \epsilon_{xy} \end{bmatrix} = \frac{1}{E} \begin{bmatrix} 1 & -\nu & -\nu & 0 & 0 & 0 \\ -\nu & 1 & -\nu & 0 & 0 & 0 \\ -\nu & -\nu & 1 & 0 & 0 & 0 \\ 0 & 0 & 0 & 1+\nu & 0 & 0 \\ 0 & 0 & 0 & 0 & 1+\nu & 0 \\ 0 & 0 & 0 & 0 & 0 & 1+\nu \end{bmatrix} \begin{bmatrix} \sigma_{xx} \\ \sigma_{yy} \\ \sigma_{zz} \\ \sigma_{yz} \\ \sigma_{zx} \\ \sigma_{xy} \end{bmatrix} \tag{9}$$

In (9), ϵ_{ij} and σ_{ij} are the strain and stress tensor components in the plane ij. The material characterization procedure followed in this paper is based on iterative substitution of the values of ν and E in the square matrix of (9) until the modal results match the experimental ones. ρ has been extracted from weight and volume of the samples.

By assuming that a solution exists of the form $\{x(t)\} = \{X\}\exp(j\omega t)$, the equation of motion becomes:

$$\left([K] - \omega^2[M]\right)\{X\} = \{0\} \tag{10}$$

This equation has the classic form of an eigenvalue problem, from which it is possible to obtain eigenvectors and eigenvalues, thus mode shapes and natural frequencies.

3 Implementation and results of the material characterization procedure

The procedure for the characterization of the material properties, described in the previous section, has been applied to a monolithic and a laminated glass sample (see sketches in Fig. 3) provided with the same material properties of the panels listed in Table 1.

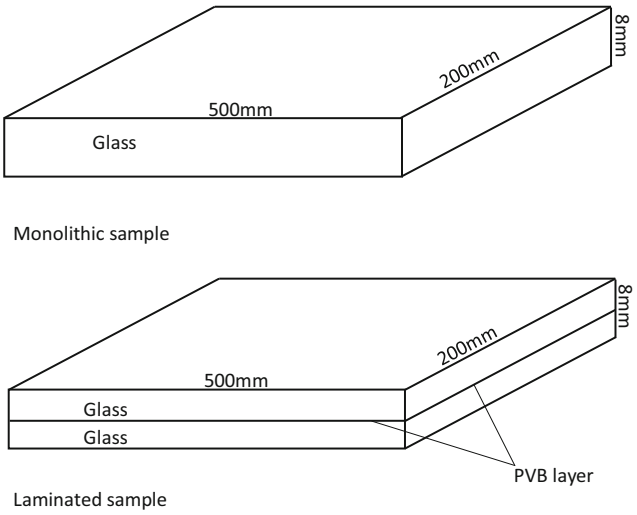

Fig. 3 Sketch of monolithic and laminated samples

Both samples have dimensions 500mm × 200mm × 8mm. For the experimental modal analysis the samples are held by a suspension system, constituted by *soft* elastic bands. These bands are designed to guarantee that the highest rigid mode frequency is less than $10-15\%$ of the first resonance frequency of the suspended structure (Kirs et al. 2018). This circumstance allows considering the systems as in *free-free* conditions.

The classical roving hammer impact test has been used to measure the frequency response functions and to implement the peak-picking method (Edwins 2003). Preliminarily, a set of points are defined on a wire-frame created on the structure and an accelerometer is fixed on one of these points. The method consists of measuring the frequency response functions between the response measured by the accelerometer and the forced excitation provided by the hammer when the wire-frame points are sequentially hit. In the present investigation, the samples have been schematized with a wire-frame consisting of 12 points displaced in adjacent rectangular patterns. An impulsive excitation has been provided, along the direction perpendicular to the plane of the structure, by means of a hammer AP Tech^{TM} AU01 provided with force transducer. The vibration response has been measured, along the same direction, by means of an ICP (Integrated Circuit Piezoelectric) mono- axial accelerometer PCB ^{TM} 353B33. The signal acquisition has been performed by a dynamic signal analyser (National Instruments ^{TM} NIcDAQ 9174 and NI 9234), controlled by PC based virtual instrument (LabVIEW ^{TM}).

Random errors have been reduced by averaging out three subsequent measurements taken for each point. The frequency response functions have been estimated as $H = S_{XY}/S_{XX}$, i.e. as the ratio of the cross-spectrum of

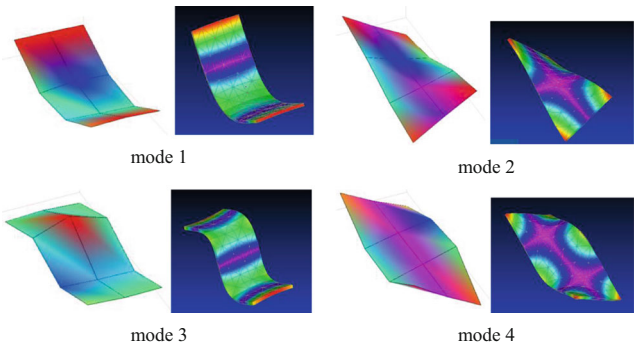

Fig. 4 Comparison between experimental and numerical modal analyses

excitation and response signals over the auto-spectrum of the excitation signal. The values of the coherence function related to the impact tests, $\gamma = |S_{XY}|^2/(S_{XX}S_{YY})$, are above 98%, indicating low levels of uncorrelated noise in the measured frequency response data. In Table 2 the experimental values found for the natural frequencies and the damping ratios are listed. The finite element modal analysis has been computed in free-free boundary conditions. Approximate material properties have been used as first attempt in the numerical model, then adjusted to fit the experimental data, as previously explained. Physically, being the mode shapes stationary waves, they are dependent only on the geometry. For this reason it is immediately possible to compare the numerical mode shapes with the experimental ones. The finite element solver used for modal analysis is ANSYS^{TM}. The test object has been discretized by means of a 3D mesh consisting of 906 nodes and 401 tetra elements.

In Fig. 4 the first four numerical and experimental modes of the two samples are shown in comparison. The *modes 1* and *2* are the first bending and the first torsional modes. The *modes 3* and *4* are the second bending and the second torsional modes. The outcomes of the material characterization process, i.e. the parameters found for the glass tempered panel and glass tempered panel with PVB, are shown in Table 3. The corresponding natural frequencies, computed with the finite element method by using these material properties, well match the experimental data, as shown in Table 4.

4 Optimization process

Once the material properties have been extracted, it has been possible to perform the second step of the procedure, i.e. the optimization process for the 16 configurations listed in Table 1. Square panels and rectangular panels have 1m × 1m and 2.50m × 0.80m sizes respectively, representing very common configurations.

Table 3 Material parameters extracted with indirect characterization based on modal analysis

Properties	Monolithic sample	Laminated sample
Young's Modulus [N/m^2]	$6.7 * 10^9$	$7.7 * 10^9$
Density [kg/m^3]	2450	2490
Poisson's Ratio	0.25	0.4

The results of the optimized solutions, in terms of averaged sound transmission loss, are compared with the ones related to the standard configurations, with the mountings placed peripherally. Through this comparison it has been possible to asses the advantages of the optimization process for each case.

The procedure has been implemented by using a software platform (ModeFrontier^{TM}), which allows to easily couple an external optimization algorithm, written in Matlab^{TM} ad-hoc for this problem, with a finite element solver (ANSYS^{TM}) and a statistical energy solver (VAOne^{TM}), according to the scheme in the Fig. 2b. We remind here that the goal of the optimization process is to find the positions of the holders which maximize the transmission loss averaged in the very low- and low- frequency ranges of investigation, 20-300 Hz and 20-1000 Hz respectively. The optimization algorithm iteratively provides new inputs for the finite element modal analysis. The positions of the holders, i.e. the design parameters, are expressed as sets of fully constrained nodes of the finite element mesh. The approach is Eulerian and the finite element mesh is fixed during the whole process. The modal results are the input for the statistical energy analysis for the evaluation of the transmission loss, which is strongly dependent on the resonance phenomena between the acoustic incident field and the panel. In particular, the modal impedance of each structural mode affects the transmission loss over the entire frequency range (Fahy 2000). The intricate dependence of the transmission loss on the holder positions motivates the use of numerical methods for this problem.

Table 4 Experimentally and numerically extracted natural frequencies

Mode number	Monolithic sample		Laminated sample	
	Experimental natural frequency	Numerical natural frequency	Experimental natural frequency	Numerical natural frequency
1	172	172	185	185
2	265	267	271	272
3	477	478	497	502
4	569	569	573	578
5	944	941	1028	1038

The optimization problem can be described in mathematical terms as:

$$\begin{aligned} &\min && f(\tau(\mathbf{x})) \quad \mathbf{x} \in \mathbb{R}^{2n} \quad n = 4, 6 \\ &\text{subject to} && \\ & && \mathbf{0} < \mathbf{x} < \mathbf{X}_c \end{aligned} \tag{11}$$

In (11), τ is the transmission factor defined in Eq. (1): $f(\tau) = 1/TL_{av}$, where TL_{av} is the averaged transmission loss $\mathrm{TL}_{av} = 1/(f_2 - 20)\int_{20}^{f_2} TL(f)df$, with $f_2 = 300$ or 1000 according to the frequency range considered. $\mathbf{x} = x_1, ..., x_{2n} = X_1, ..., X_n, Y_1, ..., Y_n$ is the generic point where τ is defined. It represents the generic set of positions of the holders, which are $(X_1, Y_1), (X_2, Y_2), ...(X_n, Y_n)$, being (X_i, Y_i) the Cartesian coordinates of the center position of the generic $i - th$ holder. The inequality constraint represents a parametric description of the areas of the panels (patches) where the holders can be placed. These patches are shown in Fig. 5. In this figure, holders with black dashed perimeter are confined in black dashed patches and holders with red dotted perimeter in red dotted patches. The patches cover the whole area in case of square panels. Instead, for rectangular panels, the holders are not allowed to be placed in the central area of the panel. This type of constraints are typically referred to as *variable bonds* (since they give lower and upper bounds for each x_i) or *box constraints* (since the feasible set is a hyperrectangle) (Boyd and Vandenberghe 2004).

Theoretically, $f(\tau(\mathbf{x}))$, (thus the TL_{av}) is a nonlinear continuous function of $\mathbf{x}$, for which the gradient based optimization techniques are particularly suitable (Sigmund and Maute 2013). However, the problem has been discretized by means of an Eulerian approach, where the positions $\mathbf{x}$ of the holders can only assume discrete

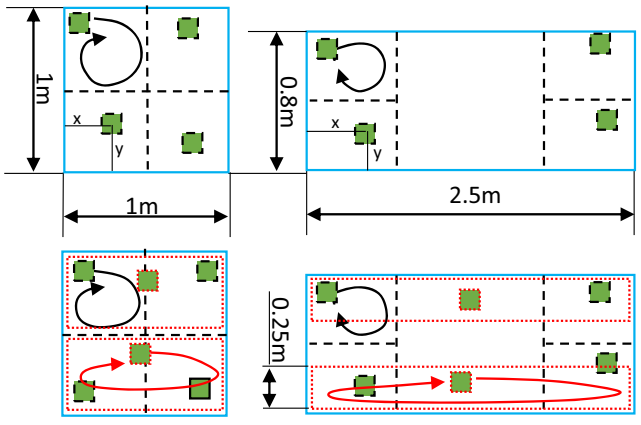

Fig. 5 Square and rectangular panel geometries, 4 and 6 holder configurations. Up-left scheme: square, 4 holders. Up-right scheme: rectangular, 4 holders. Bottom-left scheme: square, 6 holders. Bottom-right scheme: rectangular, 6 holders

Cartesian values corresponding to the nodal positions of the fixed mesh. In this way, only an approximated gradient function of $f(\tau(\mathbf{x}))$ can be computed.

In this scenario, the simplest technique for calculating the derivatives of response with respect to the design variables is the finite-difference approximation (Haftka and Gürdal 2012). In this study, the optimization procedure relies on the computation of *forward* approximations. For a given initial point $\mathbf{x}_0 = x_{1,0}, ..., x_{j,0}, ..., x_{2n,0}$, physically represented by certain positions of the holders on the plate, the closest points in the direction j is $\mathbf{x}_j = x_{1,0}, ..., x_{j,0} + d, ..., x_{2n,0}$, where d, is the distance between two consecutive nodes (a mesh with square elements has been used, thus d is constant). As a consequence, the generic component j of the function $\nabla\tau$ can be approximated as:

$$(\nabla\tau)_j \approx \frac{\tau(\mathbf{x}_0 + d\hat{\mathbf{i}}_j) - \tau(x_0)}{d} \tag{12}$$

where $\hat{\mathbf{i}}_j$ is the versor of the space with direction j. The computation of the approximate gradient allows detecting the spatial directions where the discretized objective function decreases more rapidly, i.e. the *steepest-descent* (Haftka and Gürdal 2012). For an infinitely small size mesh, this approach could be seen as a 1^{st} order method for the continuously differentiable (non-discretized) objective function $f(\tau(\mathbf{x}))$.

Once the approximate gradient has been computed in $\mathbf{x}_0$, the point $\mathbf{x}_1$ is detected by the closest-to-$\mathbf{x}_0$ nodal positions in the direction of the gradient.

Differently from optimization problems where the minima are expected to lay on constraints (e.g in structural problems where the inequalities prescribe limits on sizes, stresses, displacements, etc.), in the present investigation the inequality constraints can be removed without altering the solution. This means that constraint violations are watched by using a projection of the *box constraints* in order to keep the design parameters within the *box* (Boyd and Vandenberghe 2004).

The initial point $\mathbf{x}_0$ has been chosen by using a global polynomial approximation of the objective function. To this aim, the $f(\tau)$ has been preliminarily computed in 36 and 78 random points for the 4 holder (8 design variables) and 6 holder (12 design variables) cases, respectively. In other words, the objective function is evaluated in $n(n+1)/2$ random points (where n is the number of design variables). Thus, it is possible to obtain an acceptable polynomial approximation of the objective function according, for instance, to Haftka and Gürdal (2012). In this way, the starting point of the optimization process can be safely chosen far from local minima. This approach is particularly suitable for the problem tackled in this work, where the number of design variables is small and the computational effort required by each single optimization cycle is limited (up to two minutes on a desktop computer for the large rectangular panels). The maxima are typically reached by means of 10-20 iterations of the cycle above described (calculation of the gradient in a certain design point and move to the next design point).

A general overview of the hybrid finite element/statistical energy methodology is given in the following sub-section. The modal finite element analysis is involved in this process, but it has been discussed previously.

4.1 Hybrid FEM/SEA acoustical analysis

The Statistical Energy Analysis (SEA) is a non-deterministic energy based method whose development started in the early 1960s (Lyon and DeJong 1995). The statistical energy analysis is based on a system of linear equations, each one representing the power balance of a single subsystem of the entire system under investigation. If two subsystems i and j exchange energy, the power balance equation for the subsystem i is:

$$\Pi^i = \Pi^i_{dis} + \Pi^{ij}_{ex} \tag{13}$$

In (13) Π^i is the input power into the subsystem i, Π^i_{dis} is the dissipated power in the same subsystem and Π^{ij}_{ex} is the energy exchanged with the subsystem j. It can be shown (see Lyon and DeJong 1995) that Π^{ij}_{ex} is proportional to the difference of the total time averaged energies of subsystems, $(E_i - E_j)$ and Π^i_{dis} is proportional to E_i. As a consequence, the (13) becomes:

$$\Pi^i = \omega_c \eta_i E_i + \omega_c \eta_{ij}(E_i - E_j) \tag{14}$$

where ω_c is the angular frequency of the frequency band, η_{ij} is the coupling loss factor (CLF) and η_i and η_j are the modal densities of the two subsystems.

For the computation of the transmission loss of a plate placed between two acoustic cavities, the SEA approach consists of solving the system of linear equations of the type of (15):

$$\begin{bmatrix} \Pi_1 \\ 0 \\ 0 \end{bmatrix} = \begin{bmatrix} \eta_1 + \eta_{1p} + \eta_{12} & -\eta_{p1} & -\eta_{21} \\ -\eta_{1p} & \eta_2 + \eta_{p1} + \eta_{p2} & -\eta_{2p} \\ -\eta_{12} & -\eta_{p3} & \eta_2 + \eta_{2p} + \eta_{21} \end{bmatrix} \times \begin{bmatrix} E_1 \\ E_2 \\ E_3 \end{bmatrix} \tag{15}$$

In (15) the subscripts 1, 2 and p refer to the first, second cavities and to the plate, respectively. The transmission loss is then calculated as in (1), where the transmission factor is $\tau = p_2^2 A_2 / p_1^2 S$ and p_1 and p_2 are the pressure in the two cavities, $p_i = \rho_i c_i^2 E_i / V_i$. A_2 is the equivalent absorption area of cavity 2, $A_2 = 4\eta_i \omega_c V_i / c_i$. Finally, ρ_i, c_i, V_i are the density, the speed of sound and the volume of cavity i.

Solving the basic equation of statistical energy analysis is computationally an easy task and the method itself is fast. However, the results provided by probabilistic methods are global and no punctual information are produced such as the energy distribution in these subsystems. Another critical aspect of SEA is the estimation of the coupling factors appearing in (14) and (15). To this aim, it is possible to use a hybrid finite element method/statistical energy analysis approach, where finite element modal information are used to compute these factors (Stelzer et al. 2010; Maxit and Guyader 2001a, b).

Under the assumption of white noise excitation, let N_i and N_j be number of the the resonant modes of the subsystems i and j, respectively, in the frequency band considered. These resonant modes are chosen in a way to approximately represent the dynamic behaviour of the coupled subsystems in the frequency band considered. Every mode of each subsystem is considered not to be coupled with modes of the same subsystems but coupled with each mode of the other subsystem. In this scenario the power flow exchanged by two subsystems can be written as:

$$\Pi_{ex}^{ij} = \sum_{p=1}^{N_i} \sum_{q=1}^{N_i} \Pi_{pq}^{ij} \tag{16}$$

Π_{pq}^{ij} is the power flow between two modes on the two subsystems:

$$\Pi_{pq}^{ij} = \beta_{pq}^{ij}(E_p^i - E_q^j) \tag{17}$$

In (17) E_p^i and E_q^j are the modal energies of the mode p of the subsystem i and of the mode q of the subsystem j. β_{pq}^{ij} are called intermodal coupling loss factor (ICFs) and it can be extracted by means of modal analysis. In fact, the ICFs can be expressed as a function of the interaction modal work, the modal masses, the damping factors and the eigenfrequencies of the $p-th$ and $q-th$ mode of the subsytems i and j, as shown in Maxit and Guyader (2001b). As a consequence, the coupling loss factors of the classical statistical energy analysis can be calculated by assuming the modal equipartition of energy, as follows:

$$\eta_{ij} = \frac{1}{N_i \omega_c} \sum_{p=1}^{N_i} \sum_{q=1}^{N_i} \beta_{pq}^{ij} \tag{18}$$

Finally, by using (18), the (15) or, generally, the (14) can be solved.

5 Results of the optimization process

The results of the optimization process, including the transmission loss curves of the optimized and standard configurations, are presented in this section, which is divided into 4 parts. In Figs. 6, 9 to 12 the positions of the holders are expressed in form of relative coordinates, $(x_{rel}, y_{rel}) = (x/L_x, y/L_y)$, where x and y are the geometrical coordinates of the center node of the generic holder in a coordinate system centred at the left bottom of the panel; L_x, L_y are the horizontal and vertical size of the panel, as shown in Fig. 5. For each case examined, a sketch of the panel configuration is also included, where red squares refer to the holder positions of the standard configuration whilst green ones indicate the holder positions of the optimized configuration. A comparison between the TL_{av} of the standard and the optimized configurations is given in terms of percentage variation, $\Delta\mathrm{TL}_{av} = (\mathrm{TL}_{av-opt} - \mathrm{TL}_{av-std})/\mathrm{TL}_{av-std}$.

5.1 Square panels: 20-300 Hz

In the cases treated in this subsection, all the panels are square shaped and the very low-frequency range is in focus. The results are shown in Fig. 6.

Preliminarily, it must be pointed out that, for this type of partitions, a dip at the first resonant frequency is typically exhibited, which heavily affects the acoustic behaviour of the panel. This dip can exhibit negative values (emitting panels) (see Fig. 6a and b). Among the standard configurations, the worst overall acoustic performance is exhibited in case of monolithic with 4 holders, Fig. 6a ($\mathrm{TL}_{av} = 28.2$ dB). The standard laminated panel with 4 holders (Fig. 6c) exhibits an increase of 0.6 dB of the TL_{av} with the respect to the monolithic case. However, the advantage of the laminated solutions is the smoothing of the transmission loss curve, since the increased damping results in reduction of the vibration amplitudes, thus in more stable behaviour throughout the frequency spectrum. Higher TL_{av} values are exhibited by the standard configurations with 6 holders, with values up to 30.3 dB in both cases and typically less pronounced dips.

In the optimized configurations, the geometrical positions of the holders are moved towards the centre of the panel.

For the 4 holder cases the trend of the transmission loss is qualitatively similar to the one exhibited by the standard case, especially for the monolithic panel (Fig. 6a) where the frequencies of the first three dips are almost overlapping. However, in the optimized configurations the mode shapes undergo dramatic changes resulting in modal impedances which positively affect the transmission loss. In fact, for the monolithic 4 holder case, the increase of TL_{av}, compared to the standard cases, is $+12.1\%$.

The optimized solution for the 4 holder laminated case is characterized by the presence of a peak, following the dip of the first resonance mode, which almost overlaps the fall exhibited by the standard configuration. This

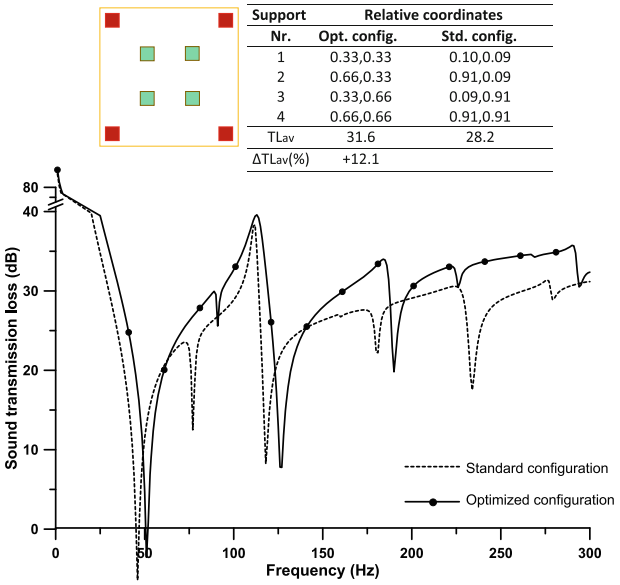

(a) Monolithic glass, square shape, 4 holders, 20-300 Hz.

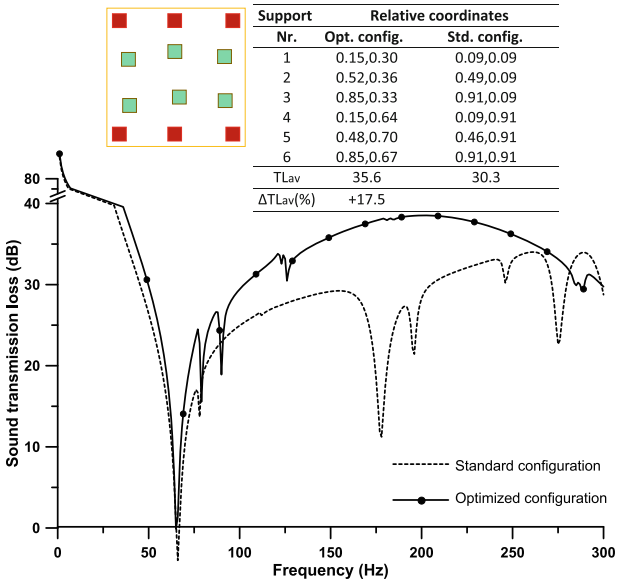

(b) Monolithic glass, square shape, 6 holders, 20-300 Hz.

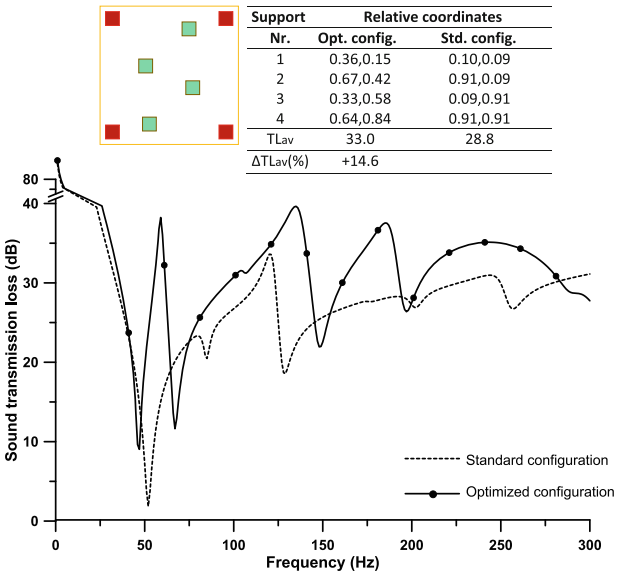

(c) Laminated glass, square shape, 4 holders, 20-300 Hz.

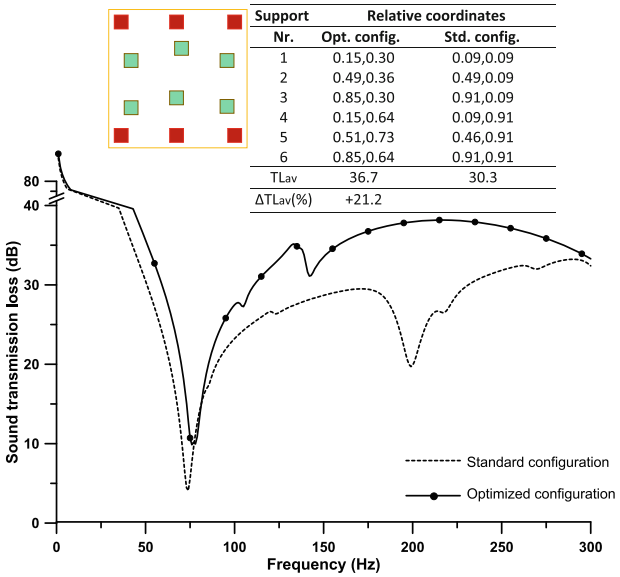

(d) Laminated glass, square shape, 6 holders, 20-300 Hz.

Fig. 6 Standard and optimized configurations for square shaped panels in frequency range 20-300 Hz. Case numbers 1, 5, 3, 7 listed in Table 1

behaviour is definitely beneficial and the increase of TL_{av}, in comparison with the standard case, is +14.6%.

The optimized solutions for the 6 holder cases (Fig. 6b and d) show similar trends, where the dips exhibited by the standard configuration in the 170-200 Hz range are not present any more. Instead a wide, regular bump occurs, ranging from 100 to 300 Hz. As expected, for the laminated case (Fig. 6d) the curve is even smoother. The increase of TL_{av} is remarkable: +17.5% and +21.2% for the monolithic and laminated cases, respectively.

As previously mentioned, positioning the holders towards the center panel has significant effects on the vibro-acoustic behaviour. In fact, in comparison with the standard case, the modal analysis shows that the central area of the optimized configurations, *stiffened* by the constraints, is nearly unaffected by modal amplitudes at low frequencies. Contrariwise, in the standard cases the whole area of the panel has non-zero modal amplitudes and it is involved in the sound transmission. This can be seen in Fig. 7a and b, where the the first mode shape of the standard and optimized

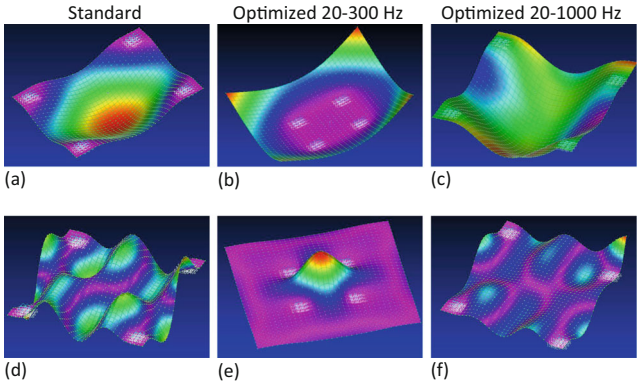

Fig. 7 Examples of mode shapes for square panels with 4 holders. Standard configuration in (**a**) and (**d**). Configuration optimized in 20-300 Hz in (**b**) and (**e**). Configuration optimized in 20-1000 Hz in (**c**) and (**f**). Details: **a** 1^{st} Mode, 52 Hz; **b** 1^{st} Mode, 48 Hz; **c** 1^{st} Mode, 47 Hz; **d** 16^{th} Mode, 368 Hz; **e** 16^{th} Mode at 391 Hz; **f** 16^{th} Mode at 358 Hz

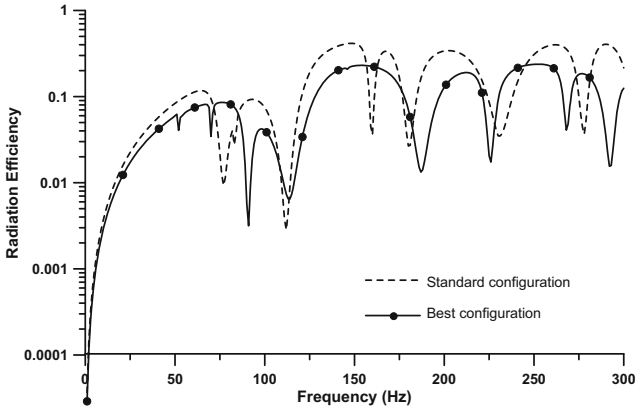

Fig. 8 Radiation efficiency for the standard and optimized panels. Case number 1

configurations for very low-frequencies is shown. In the latter case, a wide lobe in the central part of the panel is visible, while in the last case that lobe shaped mode is prevented by the presence of the holders. As a consequence, in the second case, the modal impedance of the first mode positively influences the transmission loss.

The transmitted acoustic power is proportional to the vibrating area but also to the average mean square velocity over the area ($< \bar{v^2} >= 1/S \int_S [1/T \int_0^T v^2 dt] ds$, with S panel area and T vibration period). $< \bar{v^2} >$ is related to the interaction between the stationary structural waves (i.e. the mode shapes) and the incident pressure field. As the mode shapes of the optimized configurations have normalized space-averaged amplitudes generally smaller than in case of the analogous standard configuration, the values of the space averaged velocity response is also reduced.

This aspect is supported and synthesized by the radiation efficiency parameter, calculated through statistical energy analysis. The radiation efficiency of a structure into a fluid is defined by the equation $\Pi = \rho c A < \bar{v^2} >$, where Π is the net power radiated into the fluid, ρ and c are the mass density and speed of sound in the fluid respectively, A is the structural area radiating into the fluid.

This parameter allows to highlight the response of the structure to the incident acoustic power. The higher the radiation efficiency, the higher the average mean square velocity response over the area. This implies more sensitive resonance phenomena produced by the interaction between acoustic source and structural mode shapes. In Fig. 8 the radiation efficiency is plotted for the optimized square monolithic 4 holder case and for the analogous standard case. The parameter is higher for the standard case than for the optimized case and, in correspondence of the positive picks of the radiation efficiency, the transmission loss curve shows local minima (Fig 10). Above 300 Hz, also the central part of the square cases at 300 Hz can exhibit non-zero modal amplitudes and the beneficial effect, caused by the stable central area, reduces. For this reason, other optimization cases involve the low-frequency range 20-1000 Hz.

5.2 Square panels: 20-1000 Hz

The cases included in this sub-section are related to square shaped panels in the low-frequency range. The results are shown in Fig. 9.

The most significant improvement is given by the optimized monolithic 6 holder panel (Fig. 9b), also because the transmission loss of the corresponding standard configuration shows a fairly scattered trend. By comparing the cases with and without PVB (i.e. Fig. 9a with c and b with d) it can be noticed that the presence of the interlayer generally results in smoother transmission loss trends, since the damping of the structure is increased. This fact has been already pointed out for the 20-300 Hz cases, but in the frequency range 20-1000 Hz it is even more evident. The quasi absence of dips at mid-high frequency is definitely an advantage for the laminated solutions, since it avoids isolated tones to be transmitted through the panel.

Differently from the configurations optimized in the range 20-300 Hz, the ones optimized in the range 20-1000 Hz do not overcome the high transmissibility at low frequencies. In Fig. 7c, the mode shapes at the first resonant frequency for the configuration optimized in the range 20-1000 Hz are plotted. Now the first mode is again lobe shaped, as in case of standard configuration, which negatively affects the modal impedance of this mode, thus the transmission loss. Nevertheless, the modal displacements of the first mode in

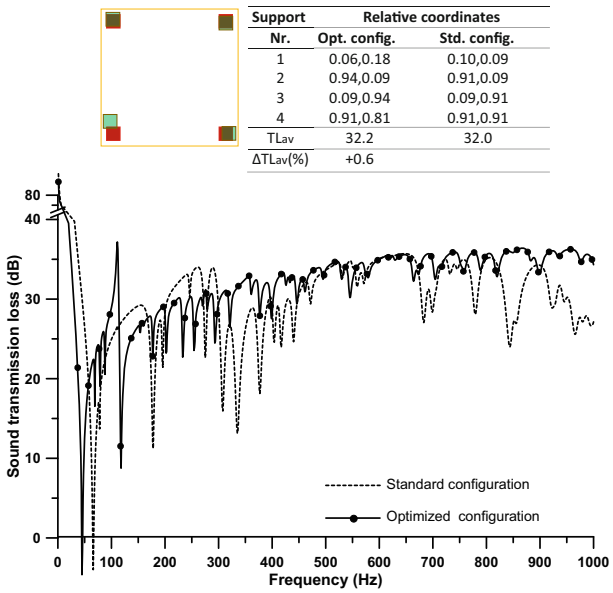

(a) Monolithic glass, square shape, 4 holders, 20-1000 Hz.

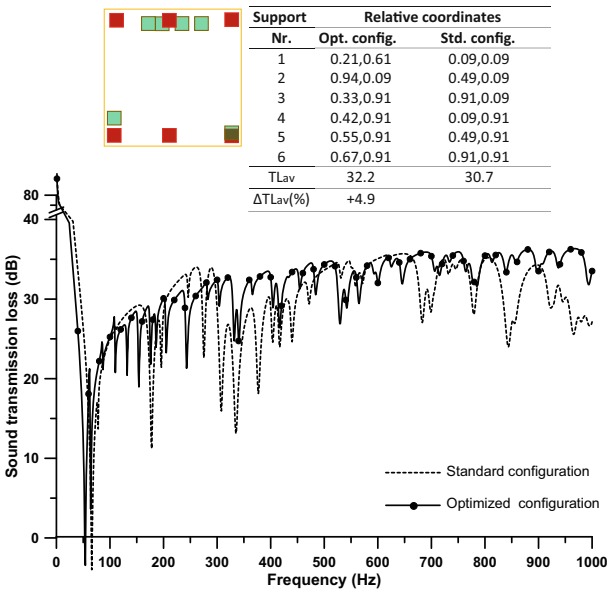

(b) Monolithic glass, square shape, 6 holders, 20-1000 Hz.

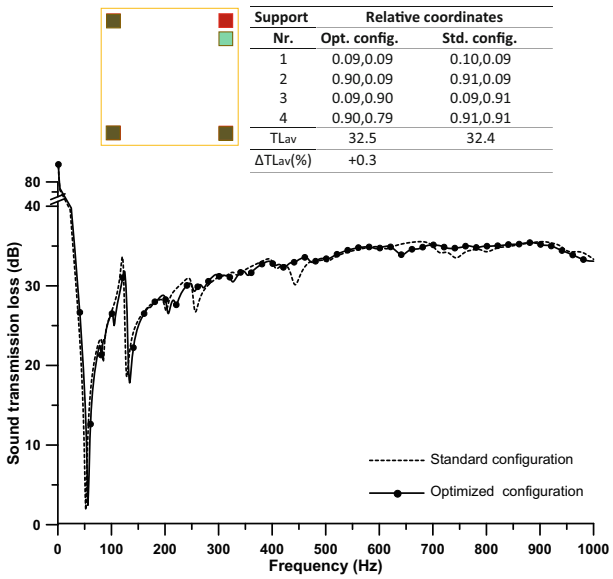

(c) Laminated glass, square shape, 4 holders, 20-1000 Hz.

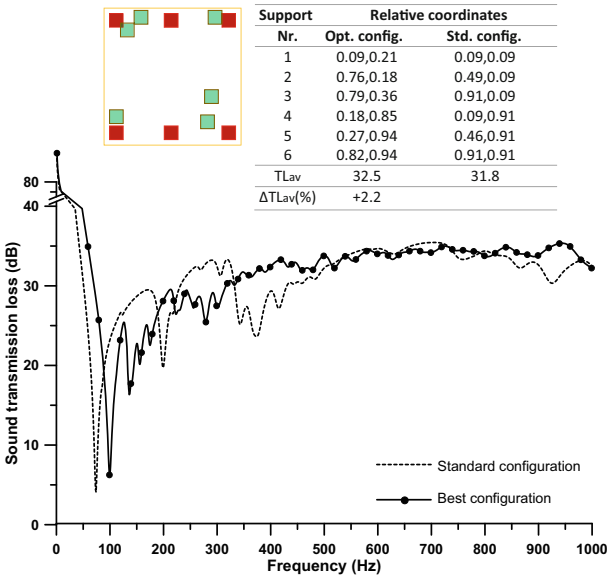

(d) Laminated glass, square shape, 6 holders, 20-1000 Hz.

Fig. 9 Standard and optimized configurations for square shaped panels in frequency range 20-1000 Hz. Case numbers 2, 6, 4, 8 listed in Table 1

the optimized configuration (Fig. 7c) are smoother than the ones in the standard configuration (Fig. 7a).

On the other hand, constraints displaced peripherally reduce the effect of higher order modes exhibited above 300 Hz, whose contribution becomes predominant when the TL_{av} is computed over the frequency range 20-1000 Hz.

This is visible in the modal shapes shown in Fig. 7d, e and f, exhibited at the 16^{th} mode by the standard configuration, by the configuration optimized in the range 20-300 Hz and by the one optimized in the range 20-1000 Hz. In the first and third case the modal amplitudes affect the hole area of the panels by means of a number of opposite lobes (bumps and basins) which often result in minor acoustic effects. Instead, in the second case, a *quasi* lobed shaped mode is generated, since one single steep bump appears at the center of the panel. As a consequence, the solution optimized in the range 20-300 Hz will possibly exhibit a dip of transmission loss at this frequency. In general, this solution is more likely to exhibit narrow band drops at frequencies higher than 300 Hz.

The condition of placing the holders peripherally is, by definition, satisfied by the standard configurations, which explains the reduced values of ΔTL_{av} shown for the 4

holder cases. However, for the 6 holder cases the optimized solutions benefit from a wider range of configurations explored by the optimizer and the performance is improved up to +4.9%.

5.3 Rectangular panels: 20-300 Hz

Since the area of the rectangular panels is 2.24 times larger than that of the square panels, the ratio between the area of the holders and the panel area reduces. As a consequence, the stiffness of the panels decreases and the modal density increases. Moreover, as visible in the sketches in Fig. 5, in case of rectangular panels the holders are confined into restricted patches which do not cover the whole area of the panel. For these two reasons, the improvement of performance of the optimized solutions is expected to be smaller than in case of square panels. Figure 10 shows that the maximum increase of transmission loss in the 20-300 Hz frequency range is exhibited by the optimized 6 holder laminated panel ($\Delta \mathrm{TL}_{av} = +8.6\%$) and the minimum increase by the optimized 4 holder monolithic panel ($\Delta \mathrm{TL}_{av} = +4.3\%$). The reduced stiffness of the structures is obviously more evident for the 4 holder cases.

By first analysing the monolithic 4 holder panels, the first mode of the standard configuration and the one of the solution optimized in the range 20-300 Hz occur at 8 and 10 Hz respectively. Naturally, having the first dip of transmission loss below 20 Hz frequency is beneficial for both the standard and the optimized configuration, since the transmission of sound occurs in non audible range.

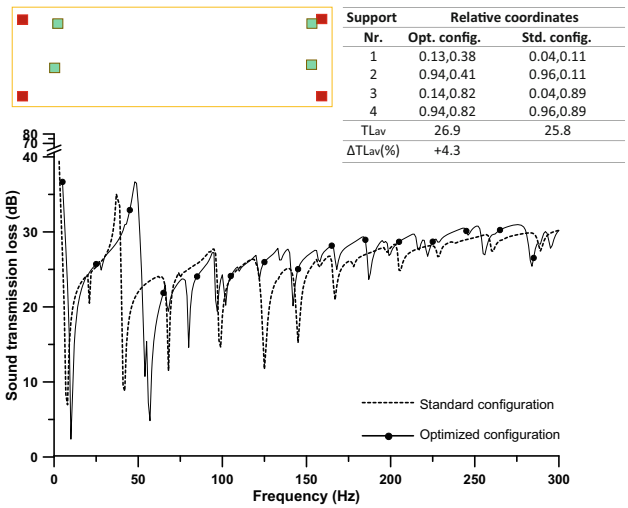

(a) Monolithic glass, rectangular shape, 4 holders, 20-300 Hz.

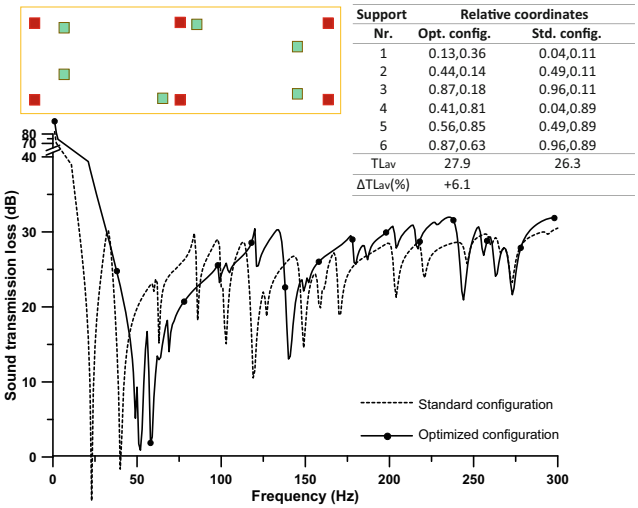

(b) Monolithic glass, rectangular shape, 6 holders, 20-300 Hz.

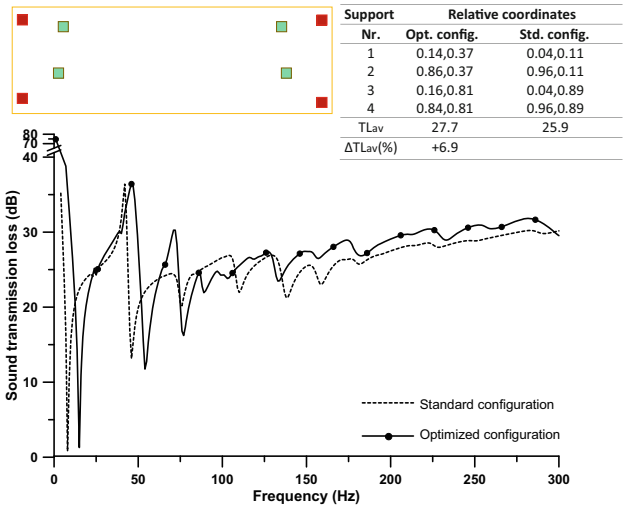

(c) Laminated glass, rectangular shape, 4 holders, 20-300 Hz.

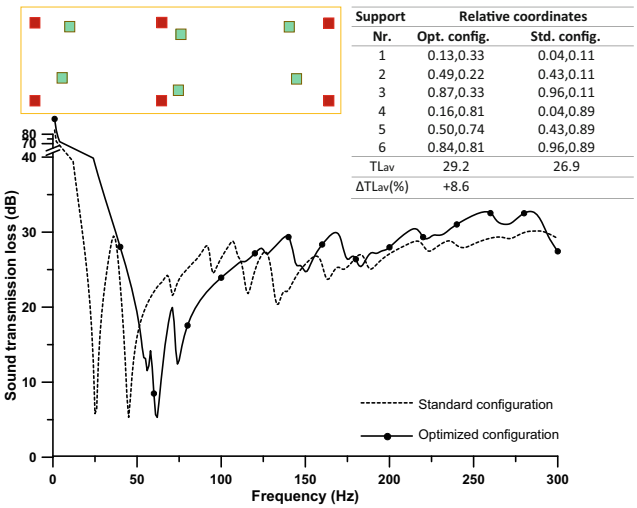

(d) Laminated glass, rectangular shape, 6 holders, 20-300 Hz.

Fig. 10 Standard and optimized configurations for rectangular shaped panels in frequency range 20-300 Hz. Case numbers 9, 13, 11, 15 listed in Table 1

The optimized configuration has the holders placed in the central part of the panel. This solution, similar to the one obtained for square panels with 4 holders, results in reduced modal amplitudes of the inner area at low frequencies. This is shown in Fig. 11a and b, where the mode shapes at 43 Hz and 58 Hz are depicted for the standard and the optimized 4 holder monolithic configurations, respectively. At these frequencies, TL minima occur but smaller relative modal amplitudes are visible for the optimized case.

For the monolithic 6 holder case the 3^{rd} mode of the standard configuration and the one of the configuration optimized in the range 20-300 Hz are shown in Fig. 11d and e. Here, the optimized positions of the holders have, not only the effect of reducing the amplitudes in the central area, but also that of rising the natural frequencies. In fact, the 3^{rd} mode occurs at 42 Hz for standard configuration and at 59 Hz for the optimized one. In general, the number of dips in transmission loss reduces in case of optimized rectangular solution and the dips are shifted towards higher frequencies, which is beneficial for the TL_{av}.

Similar considerations still hold for the laminated panels, where the $\Delta\mathrm{TL}_{av}$ is even higher, but the trend of the objective function is similar and the configurations proposed are backed by the same logic.

5.4 Rectangular panels: 20-1000 Hz

The results of the optimizations for rectangular panels in the low frequency range are shown in Fig. 12. Here the optimized solutions do not provide sensitive advantages compared to the standard configurations, especially for the 6 holder cases. Moreover, 4 and 6 holder panels present similar global acoustic perform, whilst in the previous three sets of optimizations the TL_{av} of the 6 holder panels

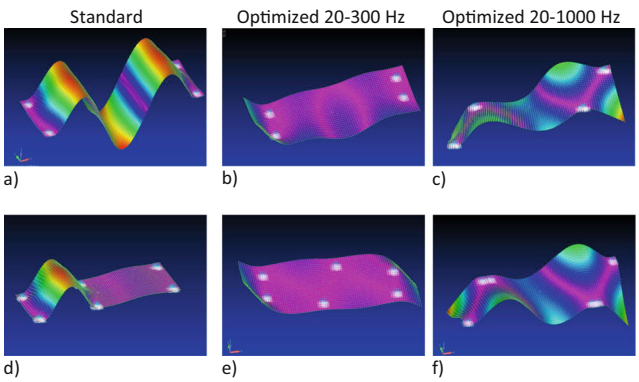

Fig. 11 Examples of mode shape examples for rectangular monolithic panels. Standard configurations in (**a**) and (**d**). Configurations optimized in 20-300 Hz in (**b**) and (**e**). Configurations opimized in 20-1000 Hz in (**c**) and (**f**). 4 holder cases in (**a**), (**b**), (**c**). 6 holder cases in (**d**), (**e**), (**f**). Details: **a** 5^{rd} mode, 43 Hz; **b** 6^{th} mode, 58 Hz; **c** 4^{th} mode, 41 Hz; **d** 3^{rd} mode, 42 Hz; **e** 6 holder case, 3^{th} mode, 59 Hz; **f** 6 holder case, 3^{th} mode, 41 Hz

was sensitively higher than that of the 4 holder panels. However, it must be pointed out that the values of TL_{av} found for the configurations examined here (included the standard ones) are among the highest found in all the cases investigated.

The optimized and standard solutions show similar TL_{av}, but the first ones present the undoubted advantage of smoother transmission loss curves, with less frequent and smaller dips. This trend is confirmed by the reduced relative modal amplitudes shown in Fig. 11c and f by both the optimized 4 and 6 holder monolithic configurations. The maximum advantage, $\Delta\mathrm{TL}_{av} = +3.1\%$, is exhibited by the second one.

6 Final remarks

As stated in Sigmund (2011), there is a limited number of cases where topological optimization problems can be efficiently tackled by using an approach based on genetic algorithm (Majak et al. 2012).

However, this is probably not the case of the problem addressed in this study. In fact, the authors have attempted to use the genetic algorithm for some of the design cases, Auriemma and Aiello (2018). It is evident that the gradient based approach is computationally more efficient and provides way more refined solutions. In fact, the number of iterations required by the method proposed in this paper is up to one order magnitude less than in case of genetic algorithm. Moreover, the minimum values found for the objective function $f(\tau(\mathbf{x}))$ are up to +40% higher and the transmission loss curves are higher and smoother, with fewer dips.

The reader could also wonder about the behaviour of the solutions optimized for 20-300 Hz when the impinging sound has wider frequency content. It has been already mentioned that these solutions can exhibit lobe shaped modes at frequency higher than 300 Hz. For this reason, tonal sound transmission must be definitely watched when solutions, optimized for very low frequency range, are used as noise barrier at frequencies higher than 300 Hz.

On the other hand, the overall behaviour of these panels can be better understood by looking at the Fig. 13. Here, the functions $TL_{av(20-f)}$ are plotted for the square panels, representing the transmission loss averaged in the frequency range 20 Hz - f, for $f \in$ [20-1000 Hz]. The cases of rectangular panels show similar trends, not reported here for brevity. The black rectangle detects the frequencies f^*up to which the $TL_{av(20-f^*)}$ of the solutions optimized for 20-300 Hz (cases 1,3,5,7,9,11,13,15) is greater than the $TL_{av(20-f^*)}$ of the solutions optimized for 20-1000 Hz (cases 2,4,6,8,10,14,16). The graph can be read by saying that the overall performance of the solutions optimized in the 20-300 Hz overcomes that of the solutions optimized

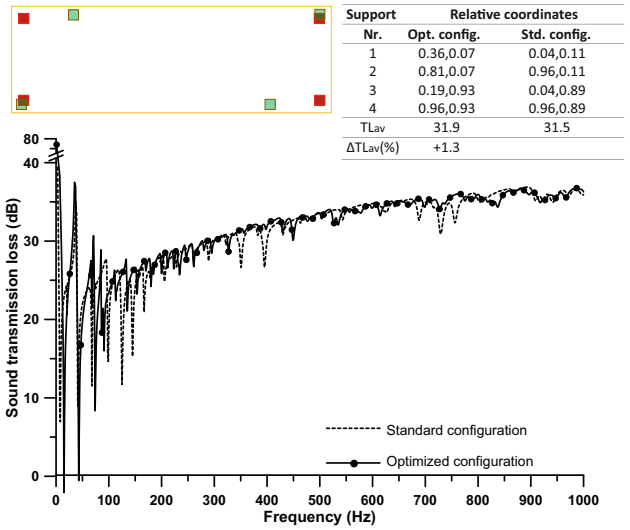

(a) Monolithic glass, rectangular shape, 4 holders, 20-1000 Hz.

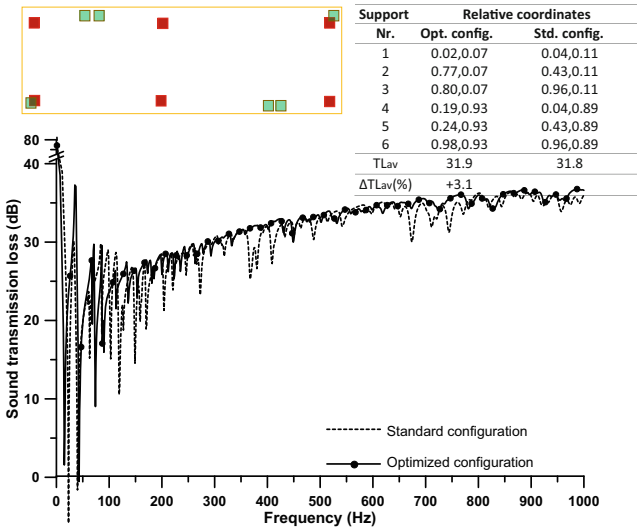

(b) Monolithic glass, rectangular shape, 6 holders, 20-1000 Hz.

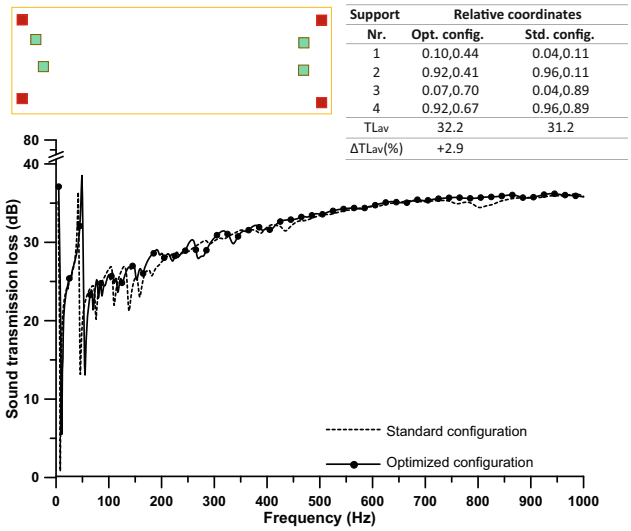

(c) Laminated glass, rectangular shape, 4 holders, 20-1000 Hz.

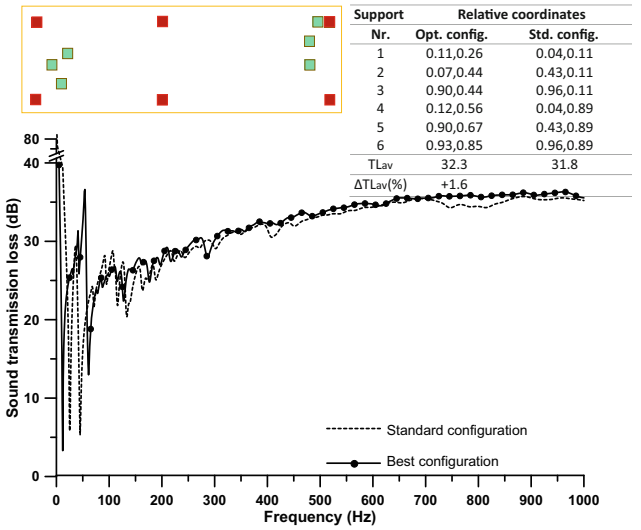

(d) Laminated glass, rectangular shape, 6 holders, 20-1000 Hz.

Fig. 12 Standard and optimized configurations for rectangular shaped panels in frequency range 20-1000 Hz. Case numbers 10, 14, 12, 16 listed in Table 1

for 20-1000 Hz up to f^*=450 Hz in the best circumstance (case 7, i.e. monolithic, square panel with 6 holders). On the other hand, the difference in $TL_{av(20-1000)}$ between the two sets of solutions is generally less than 2 dB, thus quite limited, whilst the advantage at very low frequencies of solutions optimized in the range 20-300 Hz is remarkable. As a consequence, even in environments with wider sound frequency content, if the very low frequencies are of main concern (as in most of the practical applications in room acoustics), it is worth considering solutions optimized for 20-300 Hz.

Some of the results of the optimization procedure might be aesthetically or functionally debatable. However, non vibro-acoustic considerations elude the main purpose of this investigation and they can be object of other studies. At the same time, the procedure described in this work can be easily applied to panels of suspended ceilings, even when other materials are involved, as in case of gypsum boards where the holders are typically hidden.

The suspended panels have been analysed here in baffled configurations, where the panels are surrounded by a rigid planar screen with no air gap. In this case, the motion of the unconstrained points, along direction orthogonal to the plane, is allowed. Often, in practical applications, suspended panels are glued at the periphery or embedded in structures which somehow limit the motion of the edges. As a consequence, further studies are necessary to investigate this type of boundary conditions.

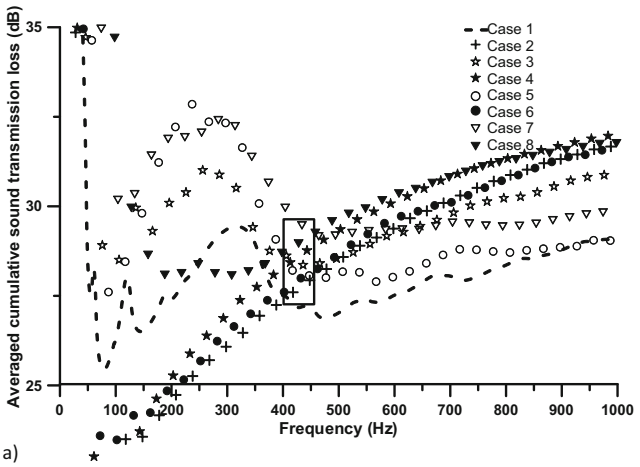

Fig. 13 Averaged cumulative transmission loss for square panels. Case numbers as listed in Table 1

7 Conclusions

In this paper, the vibro-acoustic behaviour of suspended monolithic and laminated glass panels has been studied by means of a multidisciplinary approach. It has consisted of a double step procedure. The first step has allowed to extract the material parameters of the panels (Young's modulus and Poisson's ratio) through comparison between experimental and numerical-finite element modal data. The second step has provided the optimized positions of the panel holders which maximize the sound transmission loss averaged at low- and very low- frequency ranges (20-300 Hz and 20-1000 Hz, respectively). This goal has been achieved by means of an optimization procedure based on finite difference approximation of the gradient of the objective function. The vibro-acoustic analyses have been carried out by means of hybrid finite element/statistical energy analysis.

16 different configurations have been analysed, including 2 different shapes of the panels (square and rectangular), 2 constitutive materials (monolithic glass and laminated glass with PVB interlayer), 2 holder arrangements (4 and 6 holders per panel) and the two frequency ranges above mentioned. The modal shapes, the radiation efficiency and the averaged sound transmission loss provided by the optimized and the standard configurations, where the holders are placed peripherally, have been compared.

The greatest improvements have been obtained by the solutions optimized in the range 20-300 Hz. In this case, the trend is having holders located in the central part of the panel and low values of the radiation efficiency are exhibited. With comparison to the standard configurations, the averaged transmission loss of the optimized solutions increases up to +21.2% and +8.6% for square and rectangular panels, respectively.

When the acoustic performance of the panels in the range 20-1000 Hz is of interest, the trend is moving the holders peripherally and the improvement of the performance is less sensitive. In comparison with the standard configurations, the optimized ones present more sparse and less pronounced dips in transmission loss and the problem of tonal sound transmission is reduced.

The vibro-acoustic behaviour of the solutions optimized for 20-300 Hz has been analysed also in the range 20-1000 Hz. It has been pointed out that the averaged transmission loss above 300 Hz is still acceptable, but attention must be paid to tonal transmissions which might occur above 300 Hz.

Acknowledgments This research was supported by: - Innovative Manufacturing Engineering Systems Competence Centre (IMECC) and Enterprise Estonia (EAS) and co-financed by European Union Regional Development Fund project EU48685.

Estonian Centre of Excellence in Zero Energy and Resource Efficient Smart Buildings and Districts, ZEBE, grant 2014-2020.4.01.15-0016 funded by the European Regional Development Fund.

References

Auriemma F (2017) Acoustic performance of micro-grooved elements. Appl Acoust 122:128–137. https://doi.org/10.1016/j.apacoust.2017.02.019

Auriemma F, Aiello R (2018) Optimal holder configuration of suspended glass panels. In: 25th international congress on sound and vibration, 8-12, July 2018. Hiroshima, Japan

Belegundu AD, Salagame RR, Koopman GH (1994) A general optimization strategy for sound power minimization. Struct Multidiscip Optim 8(2-3):113–119. https://doi.org/10.1007/BF01743306

Beranek LL, Work GA (1949) Sound transmission through multiple structures containing flexible blankets. J Acoust Soc Amer 21:419–428. https://doi.org/10.1121/1.1906530

Bolton JS, Shiau NM, Kang YJ (1996) Sound transmission through multi-panel structures lined with elastic porous materials. J Sound Vibr 191(3):317–347. https://doi.org/10.1006/jsvi.1996.0125

Bös J (2006) Numerical optimization of the thickness distribution of three-dimensional structures with respect to their structural acoustic properties. Struct Multidiscip Optim 32(1):12–30. https://doi.org/10.1007/s00158-005-0560-y

Boyd S, Vandenberghe L (2004) Convex optimization. Cambridge University Press. ISBN 978-0-521-83378-3

Chavan AT, Manik DN (2010) Sensitivity analysis of vibro-acoustic systems in statistical energy analysis framework. Struct Multidiscip Optim 40:283–306. https://doi.org/10.1007/s00158-009-0362-8

Cremer L (1942) Theory of the sound blockage of thin walls in case of oblique incidence. Akust Z 7:81–104

Edwins DJ (2003) Modal testing: theory, practice and application (mechanical engineering research studies: engineering dynamics series). Research Studies Press LTD, Baldock England ISBN-13: 978-0863802188

Esping B (1995) Design optimization as an engineering tool. Struct Multidiscip Optim 10(3-4):137–152. https://doi.org/10.1007/BF01742585

Fahy F (1985) Sound and structural vibration radiation, transmission and response. Edition Academic Press. ISBN 9780123736338

Fahy FJ (2000) Foundations of engineering acoustics, 1st edn. Academic Press San Diego, ISBN 0-12-247665-4

Haftka RT, Gürdal Z (2012) Elements of structural optimization, vol 11. Springer Science & Business Media

Joshi P, Mulani SB, Kapania RK (2015) Multi-objective vibro-acoustic optimization of stiffened panels. Struct Multidiscip Optim 51(4):835–848. https://doi.org/10.1007/s00158-014-1177-9

Kirs M, Karjust K, Aziz I, Ounapuu E, Tungel E (2018) Free vibration analysis of functionally graded material beam: evaluation of the haar wavelet method. Proc Estonian Acad Sci 67:1–9

Laurikis W, Mees P, Allard JF (1992) The acoustic transmission through layered systems. J Sound Vib 155:125–132. https://doi.org/10.1016/0022-460X(92)90650-M

London A (1950) Transmission of reverberant sound through double walls. J Acoust Soc Amer 22:270–279. https://doi.org/10.1121/1.1906601

Lyon RH, DeJong RG (1995) Theory and application of statistical energy analysis, 2nd edn. Butterworth-Heinemann ISBN 0-7506-9111-5

Majak J, Pohlak M, Eerme M, Velsker T (2012) Design of car frontal protection system using neural networks and genetic algorithm. Mechanika 18(4):453–460. https://doi.org/10.5755/j01.mech.18.4.2325

Maxit L, Guyader JL (2001a) Estimation of the sea coupling loss factors using dual formulation and fem modal information, part i: theory. J Sound Vibr 239:907–930. https://doi.org/10.1006/jsvi.2000.3192

Maxit L, Guyader JL (2001b) Estimation of the sea coupling loss factors using dual formulation and fem modal information, part ii: numerical applications. J Sound Vibr 235:931–948. https://doi.org/10.1006/jsvi.2000.3193

Mulholland KA, Parbrook HD, Cummings A (1967) The transmission loss of double panels. J Sound Vib 6:324–334. https://doi.org/10.1016/0022-460X(67)90205-2

Munjal ML (1993) Response of a multi-layered infinite plate to an oblique plane wave by means of transfer matrices. J Sound Vib 162:322–343. https://doi.org/10.1006/jsvi.1993.1122

Nandy AK, Jog CS (2012) Optimization of vibrating structures to reduce radiated noise. Struct Multidiscip Optim 45(5):717–728. https://doi.org/10.1007/s00158-011-0737-5

Ookura K, Saito Y (1978) Transmission loss of multiple panels containing sound absorbing materials in a random incidence field. Internoise 78:637–642

Panneton R, Atalla N (1986) Numerical prediction of sound transmission through finite multilayer systems with poroelastic materials. J Acoust Soc Amer 100:346–354. https://doi.org/10.1121/1.415956

Petyt M (1998) Introduction to finite element vibration analysis. Cambridge University Press, Cambridge. ISBN 978-0521191609

Rämmal H, Lavrentjev J (2008) Sound reflection at an open end of a circular duct exhausting hot gas. Noise Control Eng Journal 56(2):107–114. https://doi.org/10.3397/1.2898681

Siano D, Auriemma F, Bozza F (2010) Pros and cons of using different numerical techniques for transmission loss evaluation of a small engine muffler. SAE Technical Paper. https://doi.org/10.4271/2010-32-0028

Siano D, Viscardi M, Aiello R (2015) Sensitivity analysis and correlation experimental/numerical fem-bem for noise reduction assessment of an engine beauty cover. Energy Procedia 81:742–754. https://doi.org/10.1016/j.egypro.2015.12.080

Siano M, Viscardi M, Aiello R (2016) Experimental and numerical validation of an automotive subsystem through the employment of fem/bem approaches. Energy Procedia 82:67–74. https://doi.org/10.1016/j.egypro.2015.11.884

Sigmund O (2011) On the usefulness of non-gradient approaches in topology optimization. Struct Multidiscip Optim 43:589–596. https://doi.org/10.1007/s00158-011-0638-7

Sigmund O, Maute K (2013) Topology optimization approaches - a comparative review. Struct Multidiscip Optim 48:1031–1055. https://doi.org/10.1007/s00158-013-0978-6

Stelzer R, Totaro N, Pavic G, Guyader JL (2010) Prediction of transmission loss using an improved sea method. 10eme Congres Francais d'Acoustique Lyon

Tinnsten M (2000) Optimization of acoustic response — a numerical and experimental comparison. Struct Multidiscip Optim 19(2):122–129. https://doi.org/10.1007/s001580050092

Tinnsten M, Esping B (1999) Optimization of acoustic response. Struct Multidiscip Optim 18(1):36–47. https://doi.org/10.1007/BF01210690

Zargham S, Ward TA, Ramli R, Badruddin I (2016) Topology optimization: a review for structural designs under vibration problems. Struct Multidiscip Optim 53(6):1157–1177. https://doi.org/10.1007/s00158-015-1370-5

Zienkiewicz OC, Taylor RL (2000) The finite element method, volume 2: solid mechanics, 5th edn. Butterworth Heinemann. ISBN 0750650559